ELSEVIER

Remote Sensing of Environment

www.elsevier.com/locate/rse

Classification and Change Detection Using Landsat TM Data: When and How to Correct Atmospheric Effects?

Conghe Song, Curtis E. Woodcock,* Karen C. Seto,† Mary Pax Lenney,* and Scott A. Macomber**

The electromagnetic radiation (EMR) signals collected by satellites in the solar spectrum are modified by scattering and absorption by gases and aerosols while traveling through the atmosphere from the Earth's surface to the sensor. When and how to correct the atmospheric effects depend on the remote sensing and atmospheric data available, the information desired, and the analytical methods used to extract the information. In many applications involving classification and change detection, atmospheric correction is unnecessary as long as the training data and the data to be classified are in the same relative scale. In other circumstances, corrections are mandatory to put multitemporal data on the same radiometric scale in order to monitor terrestrial surfaces over time. A multitemporal dataset consisting of seven Landsat 5 Thematic Mapper (TM) images from 1988 to 1996 of the Pearl River Delta, Guangdong Province, China was used to compare seven absolute and one relative atmospheric correction algorithms with uncorrected raw data. Based on classification and change detection results, all corrections improved the data analysis. The best overall results are achieved using a new method which adds the effect of Rayleigh scattering to conventional dark object subtraction. Though this method may not lead to accurate surface reflectance, it best minimizes the difference in reflectances within a land cover class through time as measured with the Jeffries–Matusita distance. Contrary to expectations, the more complicated algorithms do not necessarily lead to improved performance of classification and change detection. Simple dark object subtraction, with or without the Rayleigh atmosphere correction, or relative atmospheric correction are recommended for classification and change detection applications.

INTRODUCTION

Two of the most common uses of satellite images are mapping landcover via image classification and landcover change via change detection. Two questions arise in all such efforts about which clear answers are not available in the literature:

1. When is atmospheric correction necessary prior to image classification and change detection?
2. If atmospheric correction is necessary, which method is best to use?

As part of a study of landuse change in the Pearl River Delta, Guangdong, China (Seto et al., 2000), we addressed these two questions. The purpose of this article is to present the results of the analyses.

The electromagnetic radiation signals collected by satellites in the solar spectrum is modified by scattering and absorption by gases and aerosols while traveling through the atmosphere from the Earth surface to the sensor. The data processing sequence for classification and change detection using remotely sensed data is illustrated in Figure 1. Each image has to go through a preprocessing step in which correction for atmospheric effects is often a primary task before classification and change detection analysis can be applied. Landsat TM

* Department of Geography, Boston, University, Boston

† Center for Environmental Science and Policy Institute for International Studies Encina Hall, Room E413 Stanford University, Stanford, C.A. 94305

Address correspondence to C. Song, Dept. of Geography, Boston Univ., 675 Commonwealth Avenue, MA 02215. E-mail: csong@crsa.bu.edu

Received 16 August 1999; revised 31 July 2000.

REMOTE SENS. ENVIRON. 75:230–244 (2001)

655 Avenue of the Americas, New York, NY 10010

0034-4257/00/$–see front matter
PII S0034-4257(00)00169-3

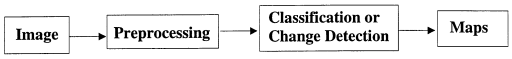

Figure 1. Data processing flow chart for classification and change detection. The remotely sensed image data are usually not ready for use directly, but need to undergo a series of preprocessing steps in which atmospheric correction is often a primary concern.

sensors have spectral bands placed in portions of the spectrum relatively unaffected by gaseous absorption in the atmosphere, and the gaseous scattering, or Rayleigh scattering, can be well characterized. However, scattering and absorption by aerosols are difficult to characterize due to their variation in time and space (Kaufman, 1993), thus constituting the most severe limitation to the radiometric normalization of satellite data (Coppin and Bauer, 1994; Liang et al., 1997).

The interaction of solar radiation with the atmosphere has been well characterized by Chandrasekhar (1960). A number of radiative transfer codes (RTCs) based on radiative transfer theory have been developed to correct for atmospheric effects in satellite images (Kneizys et al., 1988; Haan et al., 1991; Vermote et al., 1997; among others). Studies have shown that these radiative transfer codes can accurately convert the satellite measurements to surface reflectance (Holm et al., 1989; Moran et al., 1992). However, these corrections require accurate measurements of atmospheric optical properties at the time of image acquisition. These measurements are frequently unavailable or of questionable quality, which makes routine atmospheric correction of images difficult with RTCs. Many applications of remote sensing have to rely on algorithms that utilize information derived from the image itself to correct for atmospheric effects, and thus we limit our investigation to image-based correction algorithms.

Classification and Change Detection with Atmospherically Corrected Data

Depending on the application, atmospheric correction can either be absolute, where a digital number is converted to surface reflectance, or relative, where the same digital number (DN) values in corrected images represents the same reflectance, irrespective of what the actual reflectance value may be on the ground (Chavez and Mackinnon, 1994).

Dark object subtraction (DOS) is perhaps the simplest yet most widely used image-based absolute atmospheric correction approach for classification and change detection applications (Spanner et al., 1990; Ekstrand, 1994; Jakubauskas, 1996; Huguenin et al., 1997). This approach assumes the existence of dark objects (zero or small surface reflectance) throughout a Landsat TM scene and a horizontally homogeneous atmosphere. The minimum DN value in the histogram from the entire scene is thus attributed to the effect of the atmosphere and is subtracted from all the pixels (Chavez, 1989). More sophisticated algorithms derive atmospheric optical properties from dark objects in the image, and correct the images with the derived information. Ahern et al. (1977) and Gordon (1978) used clear water as the dark object to derive atmospheric optical information for radiometric normalization. More recently, Kaufman et al. (1997) found that there exist stable relationships between the surface reflectances of mid-infrared and those of the blue and red spectra for dense dark vegetation (DDV). This information can be used by atmosphere radiative transfer codes to retrieve the atmospheric optical depth which is in turned used to correct the image. Liang et al. (1997) implemented such an algorithm to correct Landsat TM images on a pixel-by-pixel basis. We included four versions of DOS approaches, the DDV approach, and a modified DDV approach in this study.

Relative atmospheric correction is based on the assumption of a linear relationship between image bands across time. The linear relationship can be determined from radiometric measurements over pseudo-invariant features (PIFs) in the images, which are objects spatially well defined and spectrally radiometrically stable. Schott et al. (1988) developed a technique that estimates the slope and intercept of the linear relationship from the mean and standard deviation of the DN values for the PIFs. Coppin and Bauer (1994) used five PIF features in three images, a clear deep oligotrophic lake, a dense mature even-aged homogeneous red pine stand, a large flat asphalt roof, an undisturbed gravel-covered area, and a concrete aircraft parking slab, to normalize Landsat images of 1984 and 1990 to the reference image of 1986 for forest cover change detection in Minnesota, USA. Pax Lenney et al. (1996) used ten Landsat TM images to monitor the status of agricultural lands in Egypt. These data were first converted to at-satellite radiances and then normalized using dark water and bright sand as the PIFs. A similar technique was applied by Michener and Houhoulis (1997) to normalize multitemporal SPOT images to monitor changes in a forest ecosystem due to flooding and by Vogelmann (1988) to monitor forest change in the Green Mountains of Vermont using multitemporal Landsat MSS images. Hall et al. (1991a) developed a radiometric rectification technique in which the PIFs are taken to be the extreme bright and dark pixels from the brightness-greenness space of the Kauth–Thomas transformation. Hall et al. (1991b) used such a method to normalize three Landsat MSS images to monitor patterns of forest succession.

Chavez and Mackinnon (1994) developed a hybrid approach which allows an absolute calibration to be applied to historical data for vegetation change detection in a desert environment. The multitemporal data were first normalized relative to a radiometric master in which

ground radiance measurements were made during satellite overpass, and then a brute-force matching was applied to render the absolute reflectance for all images.

A simpler approach taken by some other analysts to circumvent the atmospheric effects when using Landsat TM data for classification and change detection is to drop the bands that are most severely affected by the atmosphere. Foody et al. (1996) dropped both TM 1 and 2 in analysis to identify the successional stages of regenerating tropical forest. Collins and Woodcock (1994) dropped TM 1 in a study to monitor forest mortality using the Gramm-Schmidt transformation. Skole and Tucker (1993) used only TM 5 (dropped all the other bands) to monitor tropical deforestation and habitat fragmentation in the Amazon from 1978 to 1988.

An additional strategy to get around the influence of the atmosphere is to use special analysis algorithms that separate the atmospheric noise from the useful information. Fung and LeDrew (1987) used multitemporal principle component analysis for change detection without an explicit atmospheric correction in advance assuming that atmospheric differences were substantial sources of variance and they should therefore be mapped into components orthogonal to those related to landcover changes.

When Is Atmospheric Correction Needed For Classification and Change Detection?

In certain circumstances, calibration of image data to radiance units is necessary prior to classification and change detection using multitemporal images (Duggin and Robinove, 1990). The effect of the atmosphere can prevent the proper interpretation of images if it is not taken into account (Verstraete, 1994). Whether such correction is needed depends on the information desired and analytical methods used to extract the information, while choosing a correction approach should also consider the remote sensing and atmospheric data available.

For many other applications involving image classification and change detection, atmospheric correction is unnecessary. A typical example of a remote sensing application for which atmospheric correction is not necessary is image classification with a maximum likelihood classifier using a single date image. As long as the training data and the image to be classified are on the same relative scale (corrected or uncorrected), atmospheric correction has little effect on classification accuracy (Potter, 1974; Fraser et al., 1977; Kawata et al., 1990). For Landsat TM data, the dominant atmospheric effect is scattering which is additive to the remotely sensed signals, while multiplicative effect from absorption is often neglected because the TM bands were selected to avoid effects due to absorption. Thus atmospheric correction for a single date image is often equivalent to subtracting a constant from all pixels in a spectral band. Such correction is essentially nothing but translating the origins in multidimensional space as illustrated in Figure 2. Although the means of the classes change, the variance–covariance matrix remains the same regardless of correction. The unnecessary nature of atmospheric correction on classification with single date image can be extended to postclassification change detection (Singh, 1989) where multiple images are classified individually and the resulting maps are compared to identify changes (Foody et al., 1996). Similarly, atmospheric correction is also unnecessary for change detection based on classification of multidate composite imagery in which multiple dates of remotely sensed images are rectified and placed in single dataset, and then classified as if it were a single date image. In essence, as long as the training data are derived from the image being classified, atmospheric correction is unnecessary.

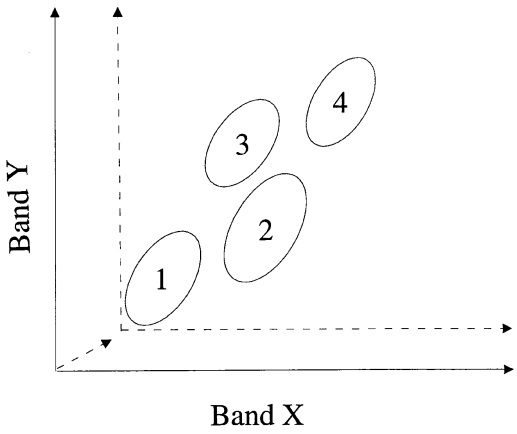

Figure 2. Subtracting a constant from a band is equivalent to translate the origin of the data set. It has no effect on the variance–covariance matrix for the classes of interest. Thus dark object subtraction for single date image have no effect on classification results.

Image differencing is another commonly used change detection technique (Singh, 1989) in which the spatially registered images from two dates are subtracted pixel by pixel. Then threshold boundaries between change and stable pixels are found for the difference image to produce the change map. Whether or not images are corrected for atmospheric effects does lead to different difference images as in Eqs. (1) and (2):

$$D'_{ijk}=[DN_{ijk}(1)-A_k(1)]-[DN_{ijk}(2)-A_k(2)], \quad (1)$$

$$D_{ijk}=DN_{ijk}(1)-DN_{ijk}(2)=D'_{ijk}+C, \quad (2)$$

where D'_{ijk} and D_{ijk} are difference images with and without atmospheric correction, respectively. $DN_{ijk}(1)$ and $DN_{ijk}(2)$ are the DNs of pixel (i, j) of dates 1 and 2 for channel k. $A_k(1)$ and $A_k(2)$ are the additive atmospheric effects of band k for dates 1 and 2. The constant C is the difference in additive atmospheric effects between two dates, $A_k(1)-A_k(2)$. The effect of atmospheric cor-

rection is equivalent to shifting the threshold values C units in the difference image histogram. In fact, the threshold boundaries are often not known *a priori*, but have to be found empirically (Jensen, 1996; Ekstand, 1994). In such circumstances, atmospheric correction can be omitted when using image difference for change detection. However, for change detection algorithms that assume a zero mean for stable classes in the difference image, radiometric normalization needs to be applied before taking the difference.

This conclusion for change detection using image differencing with regard to atmospheric correction can be extended to change detection algorithms involving general linear transformations. Collins and Woodcock (1996) compared three levels of atmospheric correction for tree mortality detection in the Lake Tahoe Basin, California, USA using multitemporal principle component analysis and a multitemporal Kauth–Thomas transformation. The three levels of atmospheric correction are 1) no correction, 2) matching DN values with PIFs, and 3) absolute correction with DOS (Chavez, 1988). The stand level tree mortality was then related to the transformed components through linear regression. Results indicate that there is no significant difference in predicting the tree mortality for the three levels of atmospheric correction using either the multitemporal principle component analysis or the multitemporal Kauth–Thomas transformation. The difference between the transformed components with and without atmospheric correction is essentially a linear transformation. The determination of the relationship between tree mortality and the spectral indices does not change with or without a linear transformation of the latter.

In contrast, it is necessary to correct atmospheric effects before classification and change detection in many other situations. The normalized difference vegetation index (NDVI) is often used to monitor vegetation dynamics (Sader, 1987; Pax Lenney et al., 1996; Michener and Houhoulis, 1997). NDVI for Landsat TM images is calculated as

$$NDVI=\frac{TM4-TM3}{TM4+TM3}. \tag{3}$$

Considering the atmospheric effects, Eq. (3) should be written as

$$NDVI=\frac{(TM4-TM3)-(A_4-A_3)}{(TM4+TM3)-(A_4+A_3)}, \tag{4}$$

where A_3 and A_4 are the additive atmospheric effects for TM 3 and TM 4, respectively. Equation (4) indicates that the atmospheric effects contaminates NDVI signals and the modification is nonlinear. Myneni and Asrar (1994) found that the NDVI at the top of the atmosphere is always smaller than that at the top of the canopy from simulations using a vegetation/atmosphere radiative transfer model. Contributions from the atmosphere to NDVI are significant (McDonald et al., 1998) and can amount to 50% or more over thin or broken vegetation cover (Verstraete, 1994). Similarly, the simple ratio (SR) vegetation index (*TM4/TM*3 for Landsat TM data) is contaminated by the atmosphere.

In general, for applications where a common radiometric scale is assumed among the multitemporal images, atmospheric correction should be taken into consideration in preprocessing. There is growing interest in monitoring large areas using remote sensing images of high spatial resolution, such as those provided by Landsat. Regional and continental scale analyses are becoming more common, or are planned for the future (Skole, 1994; MRLC, 1996; Skole et al., 1997). For applications over large areas, it would be highly beneficial to be able to train classifiers or change detection methods in one place or time, and apply them in other places and/or times. This kind of generalization will be dependent on the ability to perform routine atmospheric correction of images. In the remaining sections of this article, we present results of tests of the effects of a variety of atmospheric correction algorithms on image classification and change detection involving generalization.

ATMOSPHERIC CORRECTION METHODS

Data

The data used in this study are seven Landsat 5 TM images from 1988 to 1996 over the Pearl River Delta, Guangdong Province, China (WRS path 122 row 44). These images were assembled for a study of land-use change as this area is undergoing rapid changes due to economic development (Seto et al., 2000). The dates on which the images were collected are given as *yymmdd* as listed in Table 2. All images were coregistered to the UTM coordinate system (zone 49) with a root mean square error less than 0.3 pixels.

Dark Object Subtraction (DOS) Approaches

The relationship between the at-satellite radiance and the surface reflectance for a uniform Lambertian surface and a cloudless atmosphere can be written as (Kaufman and Sendra, 1988)

$$L_{sat}=L_p+\frac{\rho F_d T_v}{\pi(1-s\rho)}, \tag{5}$$

where L_{sat} is the at-satellite radiance, L_p is the path radiance, F_d is the irradiance received at the surface, T_v is the atmospheric transmittance from the target toward the sensor, s is the fraction of the upward radiation backscattered by the atmosphere to the surface, and ρ is the surface reflectance. The incoming irradiance at the Earth surface $F_d = E_b + E_{down}$, where E_{down} is the downwelling diffuse irradiance and E_b is the beam irradiance, E_b =

Table 1. Parameter Settings for the Four DOS Approaches Based on Eq. (6)[a]

Methods	T_v	T_z	E_{down}
DOS1	1.0	1.0	0.0
DOS2	1.0	$cos(\theta_z)$	0.0
DOS3	$e^{-\tau r/\cos(\theta_v)}$	$e^{-\tau r/\cos(\theta_z)}$	Rayleigh(6S)
DOS4	$e^{-\tau/\cos(\theta_v)}$	$e^{-\tau/\cos(\theta_z)}$	πL_p

[a] The Rayleigh atmospheric optical depth for DOS3 (τ_r) is estimated by Eq. (8), and that for DOS4 (τ) is estimated by Eq. (10). T_z for DOS2 is $\cos(\theta_z)$ for TM 1–4, and unity for TM 5 and 7.

$E_0 \cos(\theta_z)T_z$, where E_0 is the exoatmospheric solar constant, T_z the atmospheric transmittance in the illumination direction, and θ_z the solar zenith angle. Since s is small in Eq. (5), it can be neglected, and solving for ρ from Eq. (5), we get

$$\rho=\frac{\pi(L_{sat}-L_p)}{T_v(E_0\cos(\theta_z)T_z+E_{down})}. \quad (6)$$

Four DOS approaches have been included in this study, each of which calculates surface reflectance from Eq. (6) using different simplifying assumptions for T_z, T_v, and E_{down} (see Table 1).

Due to the atmospheric scattering effects, the dark object is not absolutely dark (Chavez, 1988). Assuming 1% surface reflectance for the dark objects (Chavez, 1989, 1996; Moran et al., 1992), the path radiance is estimated as

$$L_p=G\cdot DN_{min}+B-0.01[E_0\cos(\theta_0)T_z+E_{down}]T_v/\pi, \quad (7)$$

where G is the sensor gain and B the bias used for converting the sensor signals (DN) to at-satellite radiance. The effect of sensor degradation with time on G was corrected based on data by Thome et al. (1997) and Teillet et al. (2000), and the sensor biases provided by Markham and Barker (1986) were used. The minimum DN value, DN_{min}, was selected as the darkest DN with a least a thousand pixels for the entire image (Teillet and Fedosejevs, 1995; McDonald et al., 1998).

DOS1 assumes no atmospheric transmittance loss (T_v and T_z to be unity), and no diffuse downward radiation at the surface (E_{down} to be zero) in Eq. (6) (Chavez, 1989). DOS2 approximates T_z by $\cos(\theta_z)$ for TM 1–4, and unity for TM 5 and 7. Chavez (1996) showed that, for most acceptable images with atmosphere optical depth between 0.08 and 0.3, and solar zenith angle between 30° and 55°, transmittance in the illumination direction can be approximated, to a first order, by the cosine of solar zenith angle. DOS3 computes T_v and T_z assuming Rayleigh scattering only, that is, no aerosols. The optical thickness for Rayleigh scattering (τ_r) is estimated in Eq. (8) as (Kaufman, 1989)

$$\tau_r=0.008569\ \lambda^{-4}(1+0.0113\lambda^{-2}+0.00013\lambda^{-4}) \quad (8)$$

where λ is wavelength in μm. E_{down} for a Rayleigh atmosphere can be estimated by any atmospheric radiative transfer code. In this study, it was estimated by 6S (Vermote et al., 1997) for a Rayleigh atmosphere, that is, zero aerosol optical depth at 550 nm.

Finally, DOS4 attempts to add in the effects of atmospheric aerosols on T_v and T_z. For DOS4 the assumption of isotropic sky radiance is adopted here (Moran et al., 1992). With this assumption, $4\pi L_p$ estimates the amount of exoatmospheric irradiance loss. The optical thickness of the atmosphere can thus be estimated from the following equation:

$$T_z=e^{-\tau/\cos(\theta_z)}=1-\frac{4\pi L_p}{E_0\cos(\theta_z)}, \quad (9)$$

where both sides of Eq. (9) estimate atmospheric transmittance in the illumination direction. Solving for τ and substituting with Eq. (7) leads to

$$\tau=-\cos(\theta_z)\cdot\ln\times\left(1-\frac{4\pi[G\cdot DN_{min}+B-0.01(E_0\cos(\theta_z)T_z+E_{down})T_v/\pi]}{E_0\cos(\theta_z)},\right) \quad (10)$$

where E_{down} is estimated by πL_p, but T_v and T_z are unknowns before τ is estimated. We solved Eq. (10) iteratively by first setting $T_v = T_z = 1.0$. After the initial τ value was solved, new T_v and T_z can be estimated and put back in Eq. (10) to solve for another τ. This process continues until τ stabilizes, which was typically 4–5 iterations.

The Dense Dark Vegetation (DDV) Approach

The DDV approach assumes the existence of dense dark vegetation in the scene which can be used as a dark object for the blue (TM 1) and red (TM 3) channels. The Landsat TM 2.2 μm channel (TM 7) is transparent to most aerosol types (Kaufman et al., 1997). As a first-order approximation, TM 7 surface reflectance is assumed to be equal to the apparent reflectance at the top of the atmosphere. For the dense dark vegetation, Kaufman et al. (1997) found the following relationships between the surface reflectance of TM 7 and those of TM 1 and 3:

$$\rho_1=\rho_7/4, \quad \rho_3=\rho_7/2, \quad (11)$$

where ρ stands for surface reflectance and the subscripts for TM channels. The differences between the apparent reflectance in TM 1 and 3 and the predicted surface reflectance from Eq. (11) are attributed to atmospheric path radiance from which the atmospheric optical depth is estimated. Liang et al. (1997) implemented this algorithm to correct Landsat TM imagery with a "smart moving window" in which each pixel in the image was corrected according to the dense dark vegetation surface reflectance within the window or neighbouring windows.

The dense dark vegetation is identified where $\rho_7 \leqslant 0.05$ and NDVI$>$0.1.

The Modified Dense Dark Vegetation (MDDV) Approach

The DDV approach with a "smart moving window" was modified to a "fixed window" approach. Assuming uniform atmospheric condition within a Landsat TM scene, the dense dark vegetation was identified for the entire image in the same way as in DDV. The average dense dark vegetation reflectance for TM 7 was used to predict the average dense dark vegetation surface reflectance for TM 1 and 3 through Eq. (11), and the corresponding pixels were used to estimate the average apparent reflectance. To reduce the burden of data processing, the entire image was zoomed down by a factor of 10 in both vertical and horizontal directions. The 6S radiative transfer code was run iteratively for each image with midlatitude winter standard atmosphere and continental aerosol model. The aerosol optical depth for 550 nm was set to range from 0.01–2.0 with 0.01 being the step size for each iteration. The aerosol optical depth for 550 nm was determined when 6S produces a surface reflectance which matches with that predicted by Eq. (11) from the average apparent reflectance of dense dark vegetation. With this aerosol optical depth, other TM bands were corrected accordingly using 6S.

The Path Radiance (PARA) Approach

The PARA technique of Wen et al. (1999) evolved from DDV and is based on the relationship that the apparent reflectances of visible and mid-IR bands at the top of the atmosphere are linearly correlated if the surface reflectance are linearly correlated at the ground level for a horizontally homogeneous atmosphere. For Landsat TM imagery, the following relationships exist:

$$\rho_1 = \rho_1^* + \beta_1 \rho_7, \quad \rho_3 = \rho_3^* + \beta_3 \rho_7 \tag{12}$$

where β_1 and β_3 are slopes of the linear relationships and ρ_1^* and ρ_3^* are the apparent reflectance due to path radiance from which the aerosol optical depth is retrieved. To reduce the uncertainty in estimating ρ_1^* and ρ_3^*, Wen et al. (1999) used the mean apparent reflectance of homogeneous clusters of vegetation identified from TM 7. A homogeneous cluster of vegetation is defined as a 10×10 window whose standard deviation of TM 7 apparent reflectances is less than 0.02. On a graph of TM 1 or 3 versus 7, only the lower 20% of the homogeneous clusters were used to determine the linear relationships (Wen et al., 1999). The images were corrected similar to the MDDV algorithm except that the aerosol optical depth at 550 nm is estimated via 6S based on the intercept of Eq. (12).

Relative Atmospheric Correction—the Ridge Method

Relative atmospheric correction is inherently empirical and based on the assumption of a simple linear relationship among images across time and the dominance of stable features in the scene. Existing relative atmospheric correction approaches rely on the ability to identify PIFs from the images (Schott et al., 1988; Hall et al., 1991a). However, the process of PIF identification is not compatible with automatic change detection over large areas (Pax Lenney et al., 2000). Kennedy and Cohen (1998, personal communication), based on their experience, suggested use of a density plot for all the pixels in a scene with one axis being the DN value of date 1 and the other being the DN value of date 2. In such a plot, DN values of all stable features form a "ridge" with the straight line that passes along the ridge defining the relationship between dates of imagery. Each spectral band must be corrected separately.

Relative atmospheric correction does not require estimation of any atmospheric optical properties, and it corrects not only the relative difference in atmospheric conditions, but also all other perturbative factors such as sensor response and noise (Caselles and Garcia, 1989). However, when classification and change detection involve generalization in both time and space (Pax Lenney et al., 2000), relative atmospheric correction is generally not applicable because it is difficult to identifying PIFs across scenes for relative atmospheric correction. If multiple sensors are involved in the multitemporal images, it is even more complicated to apply relative atmospheric correction.

The relative atmospheric correction recommended by Kennedy and Cohen (1998, personal communication) was adopted in this study and is referred to as the Ridge Method hereafter. This method uses all information available in the image and circumvents the difficulty in identifying PIFs. The "ridge" of the density plot does not change due to minor landuse/landcover changes in the image. The image of 10 December 1988 was used as the reference image, and all other images were rescaled accordingly. Figure 3 is a density plot for TM 1 for the images of 1988 and 1989, in which the shades of grey level show differences in density. The stable components in the two images determine the ridge in the density plot. However, substantial changes in the images between two dates, such as change in phenology or land use/land cover, may compromise the utility of the Ridge Method. Fortunately, phenology does not pose a serious problem for images used in this study because all images were collected during the winter. Due to the substantial change in land use/land cover in the Pearl River Delta, this portion of the image was not used while making the density plots.

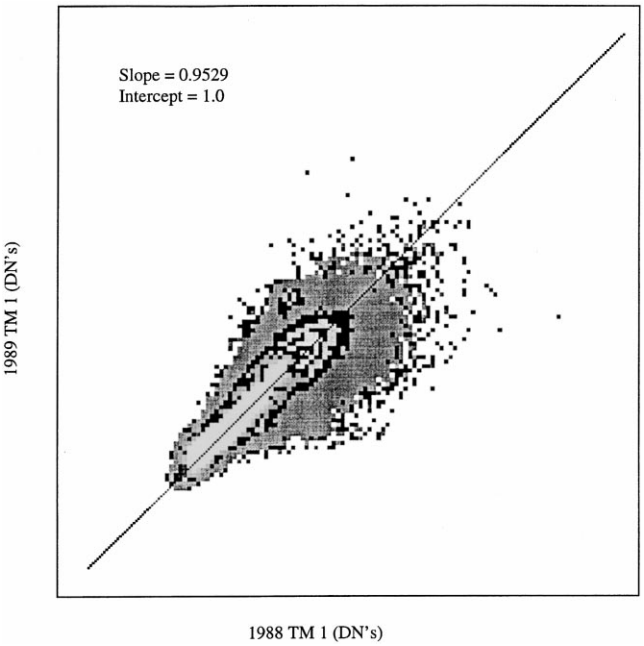

Figure 3. A density plot for TM 1 for the 1988 and 1989 images. Shades of grey level illustrate differences in density. The line that pass through the "ridge" in the center defines the relationship used to "match" the two images.

ATMOSPHERIC CORRECTION RESULTS

Atmospheric Transmittances for DOS Approaches

Transmittances in the illumination direction (T_z) for all DOS approaches for each band are plotted in Figure 4. It is unity for DOS1 for all bands across dates, and $\cos(\theta_z)$ for DOS2 for TM 1–4, which varies by date due to changes in solar zenith angle, and it is constant across bands for any given date. The transmittances are identical for DOS1 and DOS2 for TM 5 and 7. With the Rayleigh atmosphere assumption, T_z for DOS3 increases with wavelength and varies with time due to changes in solar zenith angle. For DOS4, T_z varies with both time and bands, and the estimates are lower than those for DOS3 in the visible and mid-IR bands as expected due to the consideration of aerosols. Differences among the DOS approaches for T_z diminish as the wavelength increases and converge at TM 7 where T_z is 1.

The atmospheric transmittances in the viewing direction (T_v) for all DOS approaches for each band are plotted in Figure 5. They are similar to T_z except the path length is shorter so transmissions are higher. For DOS1 and DOS2, T_v is assumed to be unity. For DOS3, it increases with wavelength, but is constant across time. It varies with both bands and time for DOS4. The differences of T_v among all DOS approaches decrease as wavelength increases and vanish at TM 7.

It is important to note that the atmospheric transmittances for DOS approaches may be different from the actual values due to the underlying assumptions. DOS1 and DOS3 certainly overestimate the transmittances in both illumination and viewing directions. DOS2 overestimates T_v. Chavez (1996) showed that $\cos(\theta_z)$ approximated T_z fairly well to a first order when the solar zenith angle is less than 55°. Since scattering by aerosols is stronger in the forward direction than in the backward direction (Forster, 1984; Kaufman, 1989), DOS4 is likely to overestimate the transmittances from the path radiance received at-satellite in the backward direction of radiation propagation. For general comparison, a midlatitude summer atmosphere with a visibility of 23 km and solar zenith angle of 55°, the transmittance in the illumination direction is about 0.40 for TM 1 and 0.90 for TM 7 (Schowengerdt, 1997). Although we do not know the true values for Figures 4 and 5, the intent is to illustrate the difference between the various approaches.

Downwelling Diffuse Irradiance at Surface and Upwelling Path Radiance Apparent Reflectance

No downwelling diffuse irradiance at the surface (E_{down}) is assumed for DOS1 and DOS2. E_{down} is obtained from 6S for DOS3, MDDV and PARA, and is estimated as πL_p for DOS4. Table 2 gives E_{down} for Landsat TM 1 for all images. The difference in E_{down} reflects the difference in the atmospheric condition accounted for by each algorithm to a certain extent. MDDV and PARA produced bigger E_{down} values than DOS3 and DOS4 did, indicating the atmosphere is estimated to be hazier by the former two approaches than the latter ones. MDDV and PARA have E_{down} values generally in the same magnitude, but DOS3 mostly has higher E_{down} values than DOS4. This implies that DOS4 underestimates E_{down} because a Rayleigh atmosphere is the clearest atmosphere possible and a real atmosphere should not lead to a lower E_{down} than DOS3 where scattering dominates.

The upwelling path radiance apparent reflectance for TM 1 is given in Table 3. The path radiance apparent reflectance for DDV varies on a pixel-by-pixel basis and are not given. Those for DOS approaches are estimated by the ratio of path radiance from Eq. (7) to the incoming solar radiance at the top of the atmosphere. The differences between the predicted surface reflectances from Eq. (11) and the observed apparent reflectances give the path radiance apparent reflectances for MDDV. The intercepts in Eq. (12) produce the path radiance apparent reflectances for PARA. The DOS approaches produce almost identical path radiance apparent reflectances, and are smaller than those from MDDV and PARA. The path radiance apparent reflectances for MDDV and PARA are equivalent in magnitude. Both the downwelling diffuse irradiance at the surface (Table 2) and the upwelling path radiance apparent reflectance suggest that MDDV and PARA consider the atmosphere hazier than DOS approaches do.

The upwelling path radiance for DDV and MDDV

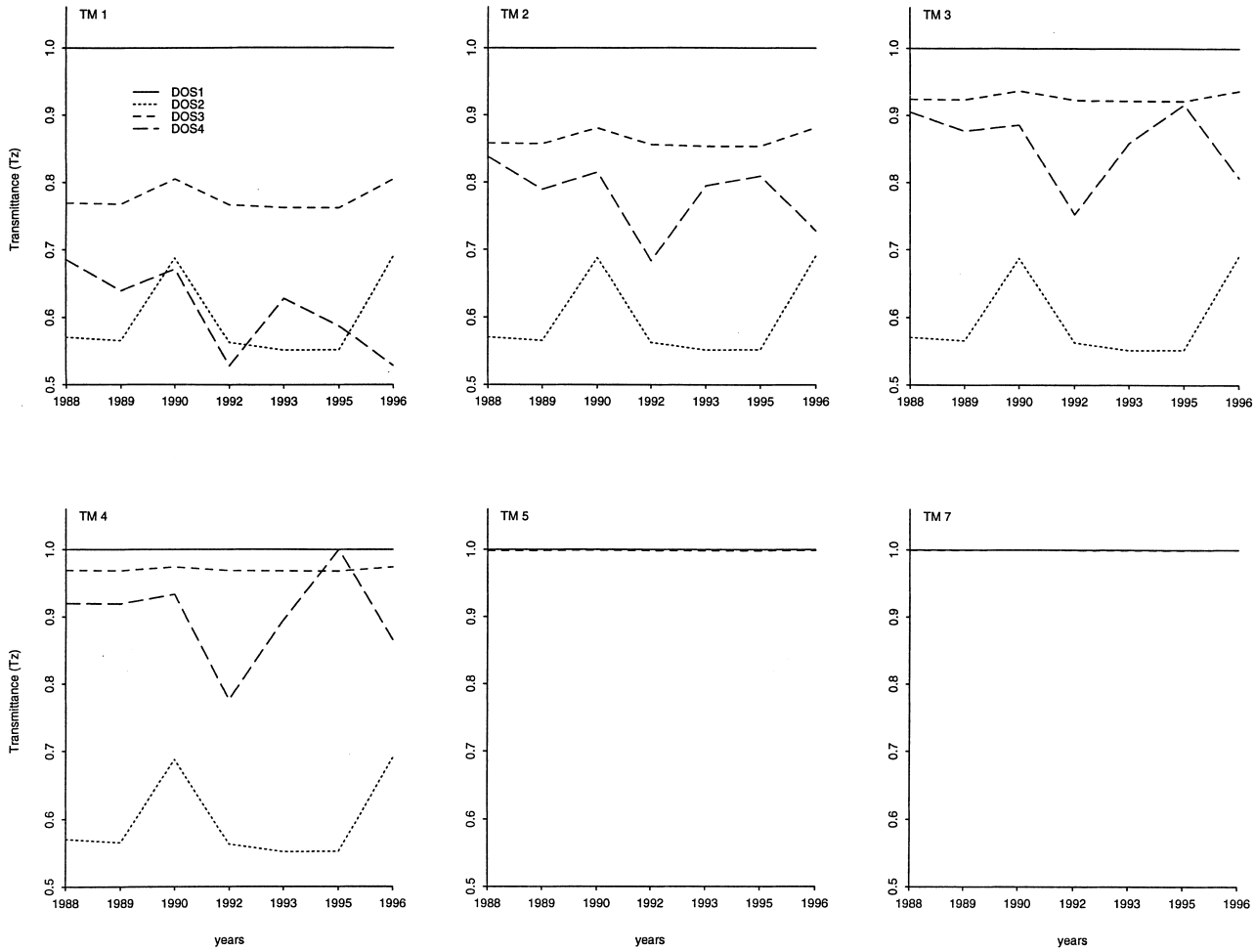

Figure 4. Atmospheric transmittance in the illumination direction (T_z) for DOS approaches for the six Landsat TM reflective channels across time.

is sensitive to the coefficients in Eq. (11). The slopes of Eq. (12) are given in Table 4 showing that β_1 and β_3 generally agree with the coefficients in Eq. (11), implying that these corrections will have similar impacts on the images to be corrected.

Raw DN to Surface Reflectance LUT

The conversion from raw DN values to surface reflectance can be processed by applying a look-up table (LUT) for algorithms assuming a horizontally homogeneous atmosphere. Among the algorithms included in this study, only DDV accounts for aerosol horizontal variation and the raw DN to surface reflectance conversion is processed for each pixel and can not be generalized to a LUT. For all other absolute atmospheric corrections, a LUT with a maximum of 256 DN levels (for 8-bit imagery) can be generated. Plotted in Figure 6 are the LUTs for the image of 1998. DOS2 generally generates the highest reflectance for a given raw DN for the visible and near-infrared bands, and its LUTs for TM 5 and 7 are identical to those for DOS1. The LUTs for DOS1 and DOS3 are very similar and so are those for MDDV and PARA. A larger range of pixels in the lower end of DN were converted to dark pixels (zero reflectance) by MDDV and PARA than DOS approaches in the visible bands. The differences among the LUTs decreased significantly at TM 5, and the LUTs were collapsed into two groups, those of DOS approaches and those of MDDV and PARA. Distinctions of LUTs between these two groups can easily be made at TM 5. But, at TM 7, there are essentially no differences among the LUTs for all the corrections.

The Effects of Atmospheric Correction on Classification and Change Detection

Classification and Change Detection Schemes

The ideal way to evaluate how accurate an atmospheric correction produces surface reflectance would be to compare *in situ* measurements of atmospheric properties and surface reflectance at the time of image acquisition with the estimates for these parameters resulting from

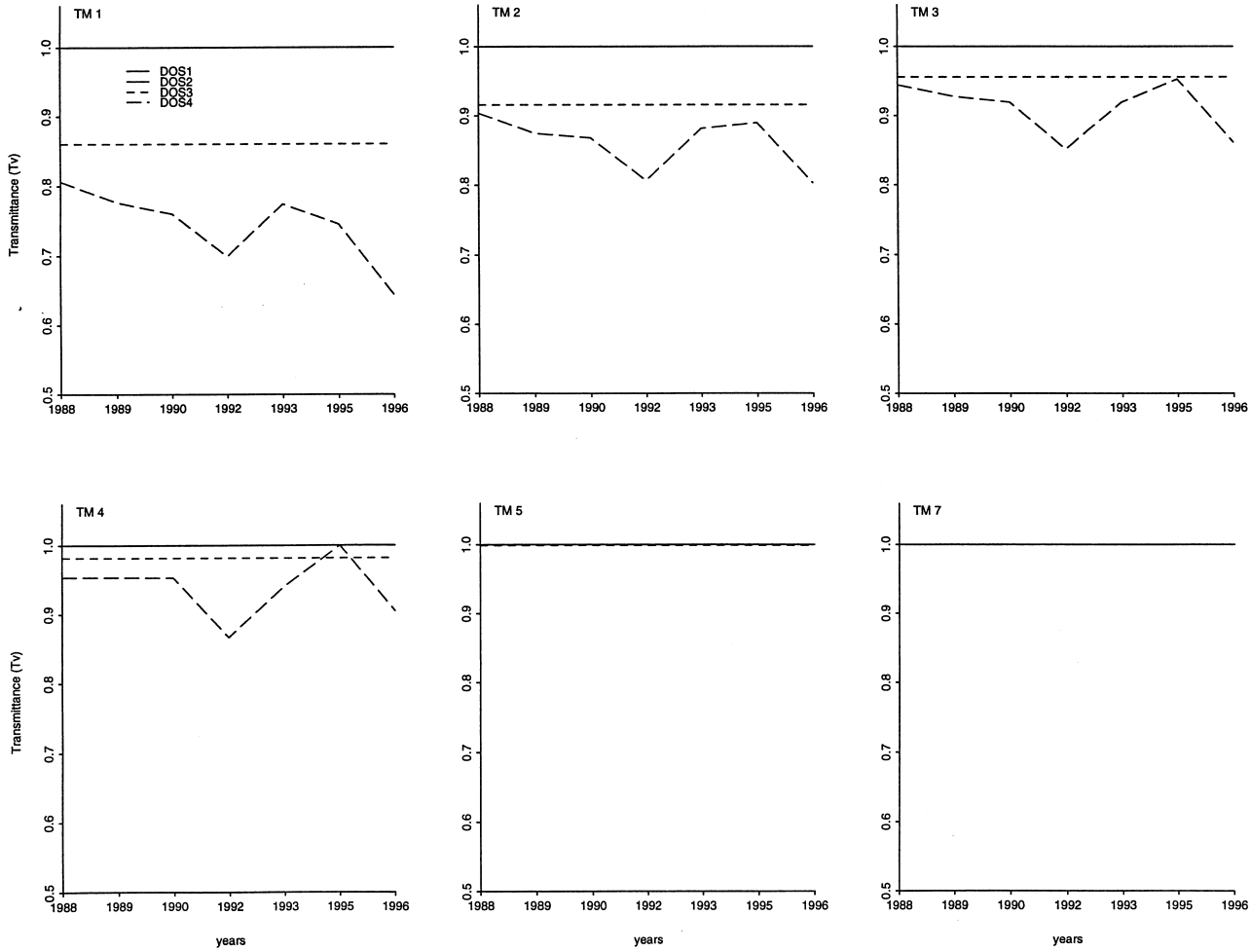

Figure 5. Atmospheric transmittance in the viewing direction (T_v) for DOS approaches for the six Landsat TM reflective channels across time.

the various forms of atmospheric correction (Holm et al., 1989; Moran et al., 1992; Ouaidrari and Vermote, 1999). Unfortunately, these measurements are not generally available, which is the case for the current dataset. However, classification and change detection do not necessarily need to be performed with absolute surface reflectance measurements, but can be performed with relative measurements as well. The key point is to maintain consistency in the measurement of surface reflectance among the multitemporal datasets, whether it is absolute or relative. Therefore, we evaluated the effect of the various atmospheric correction algorithms based on classification and change detection accuracies (Turner et al.,

Table 2. Downwelling Diffuse Irradiance of TM 1 at Surface ($W/m^2/\mu m$) for DOS3, DOS4, MDDV, and PARA Approaches[a]

Image	*DOS3*	*DOS4*	*MDDV*	*PARA*
881210	137.9	84.8	397.6	436.0
891213	137.8	97.0	446.0	408.8
901030	139.3	102.6	478.4	411.6
920120	138.1	129.8	467.6	460.2
931124	137.6	98.1	361.7	373.4
951230	137.5	110.2	411.4	409.9
960303	140.0	155.3	575.6	568.0

[a] No downwelling diffuse irradiance at the surface is assumed for DOS1 and DOS2, and it is not obtainable from the DDV code provided by Liang et al. (1997).

Table 3. The Path Radiance Apparent Reflectance of TM 1[a]

Date	*DOS1*	*DOS2*	*DOS3*	*DOS4*	*MDDV*	*PARA*
881210	0.039	0.044	0.042	0.044	0.112	0.118
891213	0.045	0.049	0.047	0.049	0.128	0.111
901030	0.059	0.062	0.061	0.063	0.108	0.092
920120	0.058	0.064	0.061	0.064	0.140	0.130
931124	0.040	0.045	0.043	0.045	0.108	0.105
951230	0.044	0.049	0.047	0.050	0.120	0.115
960303	0.082	0.085	0.085	0.088	0.139	0.129

[a] For DOS approaches, it is estimated as $\pi L_p/[E_0 \cos(\theta_0)]$. The differences between the observed apparent reflectances and the surface reflectances predicted from Eq. (11) are the path radiance apparent reflectances for MDDV, and the intercepts in Eq. (12) produce those for PARA.

Table 4. Regression Coefficients (Slopes) for Eq. (12) Using the Lower 20% of the Homogeneous Clusters with Respect to TM 7 Apparent Reflectance[a]

Date	β_1	β_3
881210	0.2184	0.4602
891213	0.2158	0.4805
901030	0.3063	0.5996
920120	0.2230	0.4356
931224	0.1614	3566
951230	0.2021	0.5740
960303	0.1641	0.3916

[a] Compare β_1 with 0.25 and β_3 with 0.5 as in Eq. (11).

1974; Fraser et al., 1977; Kawata et al., 1990; Tokola et al., 1999; Heo and FitzHugh, 2000). More specifically, we have tested the accuracies of image classifications and change detection using a maximum likelihood classifier when the training data comes from one image (or pair of images in the case of change detection) and is applied to other images. For this processing strategy to work well, atmospheric effects between dates of images must be minimized. Also, we are ultimately more interested in the accuracies of image classification and change detection than surface reflectance. The use of surface reflectance is only to provide common units applicable across space and time. While it is reasonable to expect that the method that estimates surface reflectance most accurately will also yield the most accurate image classification and change detection results, we are unable to evaluate that issue in this study.

The tests conducted involve five different situations, each using separate "ground truth" sites which are based on samples collected during field visits and augmented in number by visual interpretation of the images after returning from the field. Because the field work was based on 1988 and 1996 images, most of the testing data were collected from these images. These five tests involve different classification and change detection scenarios, and in all cases the images used for training are different from the images used for testing. Also, each of the five tests was executed in reverse order, meaning that if it was trained on image A and tested on image B,

Figure 6. Raw DN to surface reflectance LUT for absolute atmospheric corrections. No LUT for DDV can be generated because it corrects the image on a pixel-by-pixel basis.

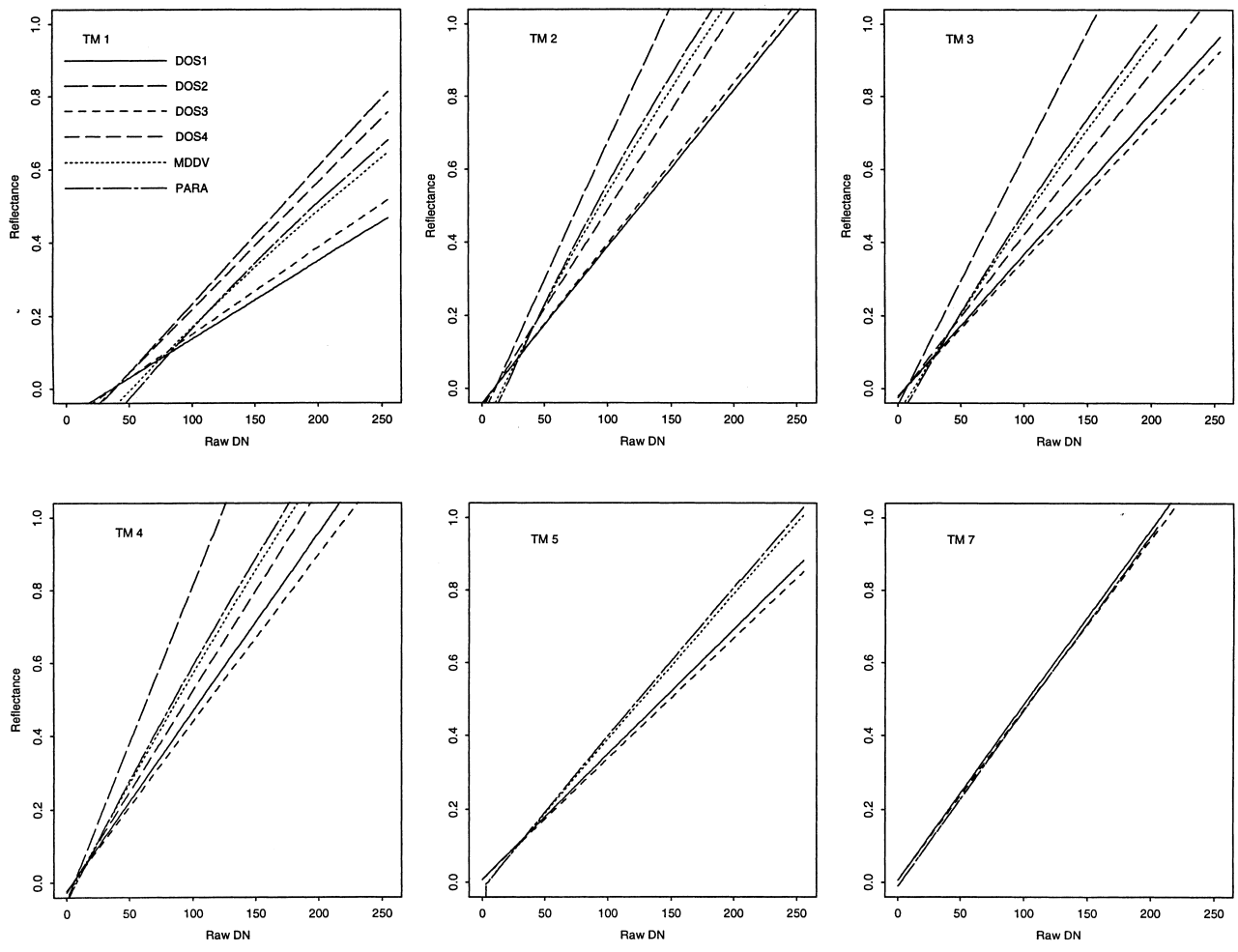

Table 5. Classification and Change Detection Accuracies (%) with Training and Testing Data Corrected by Each Atmospheric Correction Algorithm[a]

Test	*Training*	*Testing*	*Raw*	*Ridge*	*DOS1*	*DOS2*	*DOS3*	*DOS4*	*DDV*	*MDDV*	*PARA*
1	1988	1996	41 (9)	69 (1)	55 (4.5)	48 (8)	55 (4.5)	55 (4.5)	59 (2)	55 (4.5)	51 (7)
1	1996	1988	37 (9)	54 (2.5)	53 (5)	42 (8)	54 (2.5)	53 (5)	46 (7)	53 (5)	58 (1)
2	1988	1996	41 (8)	75 (2)	69 (4)	77 (1)	73 (3)	37 (9)	57 (6)	60 (5)	45 (7)
2	1996	1988	61 (9)	83 (5)	86 (2.5)	86 (2.5)	87 (1)	75 (7)	74 (8)	84 (4)	77 (6)
3	1988	1996	42 (9)	60 (5)	64 (2)	53 (7)	65 (1)	50 (8)	60 (5)	60 (5)	63 (3)
3	1996	1988	50 (9)	64 (6)	66 (5)	61 (8)	67 (3.5)	63 (7)	69 (2)	72 (1)	67 (3.5)
4	1988	1995	57 (7)	71 (1)	68 (3)	63 (5)	70 (2)	63 (5)	63 (5)	53 (8)	43 (9)
4	1995	1988	64 (6.5)	70 (5)	81 (2.5)	82 (1)	81 (2.5)	79 (4)	59 (8)	58 (9)	64 (6.5)
5	88–95	89–96	21 (9)	63 (7)	70 (3.5)	64 (6)	70 (3.5)	57 (8)	81 (1)	71 (2)	65 (5)
5	89–96	88–95	52 (9)	76 (4)	77 (2)	70 (7)	74 (6)	77 (2)	68 (8)	75 (5)	77 (2)
	Sum		(84.5)	(38.5)	(34)	(53.5)	(29.5)	(59.5)	(52)	(48.5)	(50)
	Ranks		9	3	2	7	1	8	6	4	5

[a] Numbers in parentheses indicate rank, by accuracy, for each atmospheric correction, for each test. Ranks for tied accuracies are averaged from the corresponding consecutive ranks. A lower sum of ranks indicates a better correction.

then the opposite was also done. The use of multiple tests was intended to minimize the importance of the random error component inherent in individual classification results. The overall pattern of many classifications is expected to provide a clearer indication of relative effect of the various methods.

The training and testing data for the first classification experiment were collected on the 1988 and 1996 images simultaneously. The geographical locations where the data were collected are exactly the same in the two images, but the class may have changed between dates. The classes considered are *water, fish pond, forest, urban, developing areas* (including quarries and construction sites), and *agriculture* in three stages, *early, peak,* and *harvested*.

Data for the second classification test were collected from the 1988 and 1996 images independently. Since it was easier to collect data in this test than in the first test, more data were collected. Results from the first test show that separating the agriculture into three categories causes confusion. Thus in the second test, only a single *agriculture* class was used.

The data used for the third classification is from Seto et al. (2000), which were collected from the 1988 and 1996 images simultaneously for monitoring the land use/land cover dynamics in this region. This dataset was originally intended to use as training data for an artificial network. As many examples as possible were collected for each class and a total of 809 sites were collected from the whole image. Each training site is about ten pixels in size. The classes included are the same as in the second test except for the addition of a *shrub* class.

The data used for the fourth classification were collected from the 1988 and 1995 images independently. The intention of this test was to provide some variation in the combination of solar zenith angles between the training and the testing images. The classes included in this test are identical to those in the second test.

The training and testing data for the fifth test were collected independently on the composite images of 1988–1995 and 1989–1996. This test was designed to test change detection in multidate imagery. The change classes included are *agriculture to water, agriculture to fish pond, agriculture to urban, agriculture to developing land, water to agriculture, fish pond to urban,* and *developing land to urban,* and the stable classes are *water, fish pond, forest, agriculture,* and *urban*.

Classification and Change Detection Accuracies

The overall pixel-based classification accuracies are presented in Table 5. The numbers in the parentheses are ranks of performance within a test. When the accuracies are tied, the ranks are the average of corresponding consecutive ranks. Using this approach, better correction methods have a lower sum of ranks. Tests 1–5 show that all corrections improved the classification accuracy relative to the uncorrected raw data. Among the correction algorithms, there is no single consistent "winner" over all the tests. DOS3 turns out to be the best correction method. The results for DOS1 are very similar to those of DOS3, but DOS3 results are usually better. The improvement of DOS3 over DOS1 probably results from the spectral dependence of atmospheric transmittance accounted for by DOS3 (Chavez, 1988). The Ridge Method ranks third, but its accuracies are not far from DOS3 and DOS1, indicating that it is a viable option. All other corrections occasionally perform the best, but they are inconsistent in their results and perform poorly sometimes. The performance of DDV, MDDV, and PARA are very similar because they are all based on the relationships of surface reflectances between the visible and the mid-infrared bands for dense dark vegetation. The coefficients given in Table 4 indicates that the relationships identified by PARA are very similar to those used by DDV and MDDV. There is a limited improvement of MDDV over DDV, indicating that horizontal

Table 6. Classification and Change Detection Accuracies (%) with Training and Testing Data from the Same Image(s) after Being Corrected by Each Atmospheric Correction Algorithm

Test	*Training*	*Testing*	*Raw*	*Ridge*	*DOS1*	*DOS2*	*DOS3*	*DOS3*	*DDV*	*MDDV*	*PARA*
1	1988	1988	99	99	99	99	99	99	98	99	99
1	1996	1996	96	96	96	96	96	96	96	96	96
2	1988	1988	97	97	97	97	97	97	92	96	96
2	1996	1996	97	97	97	97	97	97	95	97	97
3	1988	1988	77	77	77	77	77	77	68	77	76
3	1996	1996	82	82	82	82	82	82	77	82	82
4	1988	1988	99	99	99	99	99	99	98	99	99
4	1995	1995	89	89	89	89	89	89	87	88	88
5	88–95	89–95	100	100	100	100	100	100	98	100	100
5	89–96	88–96	99	99	99	99	99	99	96	99	96

homogeneous atmosphere is a valid assumption for the dataset used in this study.

DISCUSSION

Through scattering, atmospheric aerosols increase the apparent reflectance of dark objects and reduce it for bright objects in the image causing loss of information. The information lost cannot be recovered by these atmospheric corrections because the number of surface reflectance values or corrected DNs will not exceed the number of raw DN levels. The effects of atmospheric correction are to reduce the error in estimating the surface reflectance and/or to set a multitemporal dataset to a common radiometric scale. Atmospheric correction should not be expected to add new information to the original image. When the training and testing data are from the same image, the classification and change detection accuracies are almost identical for all the atmospheric correction methods as the raw data (Table 6). In such experiments, the training and testing data are already in a common relative scale under the assumption of a horizontally homogeneous atmosphere; thus classification and change detection is not affected by atmosphere correction. A number of previous studies showed that atmospheric correction has little effect on classification accuracy of single date image (Potter, 1974; Fraser et al., 1977; Kawata et al., 1990). Our results showed that it is unnecessary to correct atmospheric effects prior to image classification if the spectral signatures characterizing the desired classes are derived from the image to be classified. This result extends to the situations in which multidate classification is used in change detection and the multidate signatures of classes are derived from the images to be used in the multidate classification.

All the absolute correction methods used in this paper correct for effects of path radiance, which is the largest atmospheric effect on optical images (Kaufman, 1993). As a result, all these methods lead to improvements in classification and change detection when generalization is involved. The more complicated correction methods (DOS4, DDV, MDDV, PARA) try to estimate aerosol optical properties from path radiance. However, the accuracy of such estimations depends on assumptions about the reflectance of the dark objects, the aerosol single scattering phase functions, and the aerosol single scattering albedo. Classification and change detection tests indicate extraction of aerosol optical properties from path radiance for use in atmospheric correction generally does not lead to improved accuracy. Most of the time, the simple corrections (DOS3, DOS1, the Ridge Method) work best.

The results presented in this article have profound implications for the use of Landsat TM imagery to monitor large areas through time. Monitoring large areas will require movement away from the conventional approach used for studying small areas which require training data from the images to be used. Methods based on generalization of training data will be required. Since all atmospheric corrections yield improved results under these conditions, it is apparent that atmospheric correction will be a necessary component of large area monitoring proj-

Table 7. The Average Jeffries–Matusita Distance for the Same Class between Two Dates or Two Composite Dates (Test 5)[a]

Test	*Raw*	*Ridge*	*DOS1*	*DOS2*	*DOS3*	*DOS4*	*DDV*	*MDDV*	*PARA*
1	1.99	1.79	1.85	1.91	1.80	1.96	1.93	1.90	1.89
2	1.98	1.28	1.60	1.84	1.46	1.88	1.73	1.72	1.77
3	1.89	1.11	1.32	1.65	1.18	1.59	1.29	1.46	1.35
4	1.85	1.84	1.80	1.85	1.83	1.79	1.84	1.79	1.90
5	1.99	1.97	1.93	1.95	1.95	1.97	1.91	1.91	1.89

[a] DOS3, DOS1 and Ridge Method have shorter JM distances which generally corresponds to higher accuracies in Table 5. Note the JM distance for Test 5 is on a different scale due to the increase in dimensions.

ects. Our results of the simpler methods producing the best results is encouraging with regard to the processing constraints associated with analyzing large numbers of Landsat images.

This evaluation based on classification and change detection accuracies does not provide information about which absolute atmospheric correction results in the most accurate estimates of surface reflectance, but about how well a multitemporal dataset was brought to a common scale by an atmospheric correction. The average Jeffries–Matusita (JM) (Richards, 1993) distance for the same class between dates for the five tests are given in Table 7. The smaller the JM distance, the "closer" the same class is to itself spectrally on different dates after atmospheric correction. Thus, a good method for atmospheric correction minimizes the spectral distance between dates for the same class, leading to lower JM distance values. The relative magnitude of the JM distance values in Table 7 generally agrees with the classification accuracy in Table 5. DOS3, DOS1, and the Ridge Method did a better job in bringing the multidate images to a common scale than the other methods. When viewed from this perspective, the methods most effective for image preprocessing in support of classification and change detection need not be the most effective for estimating surface reflectance.

CONCLUSIONS

Atmospheric correction is not always necessary for classification and change detection. Both simple theoretical analysis and empirical results indicate that only when training data from one time or place are applied in another time or place is atmospheric correction necessary for image classification and many change detection methods. Seven absolute and one relative atmospheric corrections were evaluated with respect to their impacts on image classification and change detection accuracies involving generalization. All corrections improved the accuracies. For classification and change detection involving generalization in time and/or space to perform well, it is important that the radiometric measurements be set on a common relative scale, but accurate estimation of surface reflectance is not necessary. The best overall results are achieved with a new method which adds the effect of Rayleigh scattering to conventional dark object subtraction. Contrary to expectations, the recently developed methods of atmospheric correction which are more complicated do not lead consistently to improved classification and change detection accuracies relative to the simpler ones. Though the simpler atmospheric correction algorithms may not be as accurate as the more complicated ones in estimating surface reflectance, they do a better job of reducing the differences due to atmospheric effects between multidate images as measured by JM distance. For applications where surface reflectances are not required, simple atmospheric correction algorithms, such as DOS or a relative correction, is recommended. Further studies are needed to evaluate which image-based correction algorithm leads to the most accurate estimates of surface reflectance.

This research is partly supported by NASA Grant NAG5-3439 and partly supported by NASA Grant NAG5-6214. The authors wish to thank Dr. Yoram J. Kaufman for thoughtful discussion; Dr. Shunlin Liang for providing the code for DDV; Dr. Guoyong Wen for communications regarding using PARA to correct images; and Dr. Philippe M. Teillet for providing the sensor degradation calibration data including the most recent cross-calibration data between Landsat 5 and 7. The authors are also grateful for inputs from the anonymous reviewers.

REFERENCES

Ahern, F. J., Goodenough, D. G., Jain, S. C. Rac, V. R., and Rochon, G. (1977), Use of clear lakes as standard reflectors for atmospheric measurements. In *Proceedings of the 11th International Symposium on Remote Sensing of Environment*, Ann Arbor, MI, pp. 731–775.

Caselles, V., and Garcia, M. J. L. (1989), An alternative simple approach to estimate atmospheric correction in multitemporal studies. *Int. J. Remote Sens.* 10:1127–1134.

Chandrasekhar, S. (1960), *Radiative Transfer*, Dover, New York.

Chavez, P. S., Jr. (1988), An improved dark-object subtraction technique for atmospheric scattering correction of multispectral data. *Remote Sens. Environ.* 24:459–479.

Chavez, P. S., Jr. (1989), Radiometric calibration of Landsat Thematic Mapper multispectral images. *Photogramm. Eng. Remote Sens.* 55:1285–1294.

Chavez, P. S., Jr. (1996), Image-based atmospheric corrections-revisited and improved. *Photogramm. Eng. Remote Sens.* 62: 1025–1036.

Chavez, P. S., Jr., and Mackinnon, D. J. (1994), Automatic detection of vegetation changes in the southwestern United States using remotely sensing images. *Photogramm. Eng. Remote Sens.* 60(5):571–583.

Collins, J. B., and Woodcock, C. E. (1994), Change detection using the Gramm–Schmidt transformation applied to mapping forest mortality. *Remote Sens. Environ.* 50:267–279.

Collins, J. B., and Woodcock, C. E. (1996), An assessment of several linear change detection techniques for mapping forest mortality using multitemporal Landsat TM data. *Remote Sens. Environ.* 56:66–77.

Coppin, P. R., and Bauer, M. E. (1994), Processing of multitemporal Landsat TM imagery to optimize extraction of forest cover change features. *IEEE Trans. Geosci. Remote Sens.* 32(4):918–927.

Duggin, M. J., and Robinove, C. J. (1990), Assumptions implicit in remote sensing data acquisition and analysis. *Int. J. Remote Sens.* 11:1669–1694.

Ekstrand, S. (1994), Assessment of forest damage with Landsat TM: correction for varying forest stand characteristics. *Remote Sens. Environ.* 47:291–302.

Foody, G. M., Palubinska, G., Lucas, R. M, Curran, P. J., and Honzak, M. (1996), Identifying terrestrial carbon sinks: clas-

sification of successional stages in regenerating tropical forest from Landsat TM data. *Remote Sens. Environ.* 55:205–216.

Forster, B. C. (1984), Derivation of atmospheric correction procedures for Landsat MSS with particular reference to urban data. *Int. J. Remote Sens.* 5:799–817.

Fraser, R. S., Bahethi, O. P., and Al-Abbas, A. H. (1977), The effect of the atmosphere on the classification of satellite observation to identify surface features. *Remote Sens. Environ.* 6:229–249.

Fung, T., and LeDrew, E. (1987), Application of principle components analysis to change detection. *Photogramm. Eng. Remote Sens.* 53(12):1649–1658.

Gordon, H. R. (1978), Removal of atmospheric effects from satellite imagery of the ocean. *Appl. Opt.* 17:1631–1636.

Haan, J. F., Hovenier, J. W., Kokke, J. M. M., and Stokkom, H. T. C. (1991), Removal of atmospheric influences on satellite-borne imagery: a radiative transfer approach. *Remote Sens. Environ.* 37:1–21.

Hall, F. G., Strebel, D. E., Nickeson, J. E., and Goets, S. J. (1991a), Radiometric rectification: toward a common radiometric response among multidate, multisensor images. *Remote Sens. Environ.* 35:11–27.

Hall, F. G., Botin, D. B., Strebel, D. E., Woods, K. D., and Goets, S. J. (1991b), Large-scale patterns of forest succession as determined by remote sensing. *Ecology* 72:628–640.

Heo, J., and FitzHugh, W. (2000), A standardized radiometric normalization method for change detection using remotely sensed imagery. *Photogramm. Eng. Remote Sens.* 66:173–181.

Holm, R. G, Jackson, R. D., Yuan, B., Moran, M. S., Slater, P. N., and Bigger, S. F. (1989), Surface reflectance factor retrieval from Thematic Mapper data. *Remote Sens. Environ.* 27:47–57.

Huguenin, R. L., Karaska, M. A., Blaricom, D. V., and Jensen, J. R., (1997), Subpixel classification of bald cypress and tupelo gum trees in Thematic Mapper imagery. *Photogramm. Eng. Remote Sens.* 63(6):717–725.

Jakubauskas, M. E. (1996), Thematic mapper characterization of Lodgepole pine seral stages in Yellowstone Nationa Park, USA. *Remote Sens. Environ.* 56:118–132.

Jensen, J. R. (1996), *Introductory Digital Image Processing: A Remote Sensing Perspective,* Prentice-Hall, Englewood Cliffs, NJ.

Kaufman, Y. J. (1989), The atmospheric effect on remote sensing and its correction. In *Theory and Application of Optical Remote Sensing* (G. Asrar, Ed.), New York, pp. 341ff.

Kaufman, Y. J. (1993), Aerosol optical thickness and atmospheric path radiance. *J. Geophys. Res.* 98:2677–2692.

Kaufman, Y. J., and Sendra, C. (1988), Algorithm for automatic atmospheric corrections to visible and near-IR satellite imagery. *Int. J. Remote Sens.* 9:1357–1381.

Kaufman, Y. J., Wald, A., Remer, L. A., Gao, B., Li, R., and Flynn, L. (1997), The MODIS 2.1 μm channel—correlation with visible reflectance for use in remote sensing of aerosol. *IEEE Trans. Geosci. Remote Sens.* 35:1–13.

Kawata, Y., Ohtani, A., Kusaka, T., and Ueno, S. (1990), Classification accuracy for the MOS-1 MESSR data before and after the atmospheric correction. *IEEE Trans. Geosci. Remote Sens.* 28:755–760.

Kneizys, F. X., Shettle, E. P., and Gallery, W. O., et al. (1988), Atmospheric transmittance/radiance: computer code LOWTR4AN-7 AFGL-TR-88-0177, Air Force Geophysics Lab, Hanscom AFB, MA.

Liang, S., Fallah-Adl, H., Kalluri, S., JaJa, J., Kaufman, Y. J., and Townshend, J. R. G. (1997), An operational atmospheric correction algorithm for Landsat Thermatic Mapper imagery over the land. *J. Geophys. Res.* 102:17,173–17,186.

Markham, B. L., and Barker, J. L. (1986), Landsat MSS and TM post-calibration dynamic ranges, exoatmospheric reflectance and at-satellite temperature, EOSAT Landsat Technical Notes.

McDonald, A. J., Gemmell, F. M., and Lewis, P. E. (1998), Investigation of the utility of spectral vegetation indices for determining information on coniferous forests. *Remote Sens. Environ.* 66:250–272.

Michener, W. K., and Houhoulis, P. F. (1997), Detection of vegetation changes associated with extensive flooding in a forested ecosystem. *Photogramm. Eng. Remote Sens.* 63: 1363–1374.

Moran, M. S., Jackson, R. D., Slater, P. N., and Teillet, P. M. (1992), Evaluation of simplified procedures for retrieval of land surface reflectance factors from satellite sensor output. *Remote Sens. Environ.* 41:169–184.

MRLC (1996), Implementation strategy for an MRLC national 30m land cover data base, MRLC Consortium Documentation, http://www.epa.gov/mrlc/About.html.

Myneni, R. B., and Asrar, G. (1994), Atmospheric effects and spectral vegetation induces. *Remote Sens. Environ.* 47: 390–402.

Ouaidrari, H., and Vermote, E. F. (1999), Operational atmospheric correction of Landsat data. *Remote Sens. Environ.* 70:4–15.

Pax Lenney, M., Woodcock, C. E., Collins, J. B., and Hamdi, H. (1996), The status of agricultural lands in Egypt: the use of multitemporal NDVI features derived from Landsat TM. *Remote Sens. Environ.* 56:8–20.

Pax Lenney, M., Woodcock, C. E., Gopal, S., and Macomber, S. A. (2000), Monitoring temperate conifer forests with Landsat TM: a new look at classification generalization. *Remote Sens. Environ.*, in press.

Potter, J. F. (1974), Haze and sun angle effects on automatic classification of satellite data-simulation and correction. *Proc. Soc. Photo-Opt. Instrum. Eng.* 51:73–83.

Richards, J. A. (1993), *Remote Sensing Digital Image Analysis: An Introduction,* Springer-Verlag, New York, 250 pp.

Sader, S. A. (1987), Digital image classification approach for estimating forest clearing and regrowth rates and trends. In *International Geoscience and Remote Sensing Symposium*, Ann Arbor, Michigan, 18–21 May, pp. 209–213.

Schott, J. R., Salvaggio, C., and Volchok, W. J. (1988), Radiometric scene normalization using pseudoinvariant features. *Remote Sens. Environ.* 26:1–16.

Schowengerdt, R. A. (1997), *Remote Sensing: Models and Methods for Image Processing,* Academic, San Diego.

Seto, K. C., Woodcock, C. E., Song, C., Huang, X., Lu, J., and Kaufmannn, R. K. (2000), Monitoring land-use change in the Pearl River Delta using Landsat TM. *Int. J. Remote Sens.*, in press.

Singh, A. (1989), Digital change detection techniques using remotely-sensed data. *Int. J. Remote Sens.* 10:989–1003.

Skole, D. L., (1994), Data on global land cover change: acquisition, assessment, and analysis. In *Global Land Cover and*

Land Use Change, (W. B. Meyer, and B. L. Turner, Eds.), Cambridge University Press, Cambridge.

Skole, D., and Tucker, C. (1993), Tropical deforestation and habitat fragmentation in the Amazon: satellite data from 1978 to 1988. *Science* 260:1905–1910.

Skole, D. L., Justice, C. O., Townshend, J. R. G., and Janetos, A. C. (1997), A land cover change monitoring program: strategy for an international effort. *Mitigation Adaptation Strategies Global Change* 2:157–175.

Spanner, M. A., Pierce, L. L., Peterson, D. L., and Running, S. W. (1990), Remote sensing of temperate coniferous forest leaf area index: the influence of canopy closure, understory vegetation and background reflectance. *Int. J. Remote Sens.* 11(1):95–111.

Teillet, P. M., and Fedosejevs, G. (1995), On the dark target approach to atmospheric correction of remotely sensed data. *Can. J. Remote Sens.* 21:373–387.

Teillet, P. M., Markham, B. L., Barker, B. L., Storey, J. C., Irish, R. R., and Seiferth, J. C. (2000), Landsat sensor cross-calibration using nearly-coincident matching scenes: In *Proceedings of the SPIE conference on Algorithms for Multispectral, Hyperspectral, and Ultraspectral Imagery VI*, SPIE Vol. 4049, Orlando, FL, in press.

Thome, K., Markham, B., Barker, J., Slater, P., and Biggar, S. (1997), Radiometric calibration of Landsat. *Photogramm. Eng. Remote Sens.* 63:853–858.

Tokola, T., Lofman, S., and Erkkila, A. (1999), Relative calibration of multitemporal landsat data for forest cover change detection. *Remote Sens. Environ.* 68:1–11.

Turner, R. E., Malila, W. A., Nalepka, R. F., and Thomson, F. J. (1974), Influence of the atmosphere on remotely sensed data. *Proc. Soc. Photo-Opt. Instrum. Eng.* 51:101–114.

Verstraete, M. (1994), The contribution of remote sensing to monitor vegetation and to evaluate its dynamic aspects. In *Vegetation, Modeling and Climatic Change Effects*, (F. Veroustraete, R. Ceulemans, et al., Eds.), SPB Academic Publishing, The Hague, The Netherlands. pp. 207–212.

Vermote, E. F., Tanré, D., Deuze, J. L., Herman, M., and Morcrette, J. J. (1997), *Second Simulation of the Satellite Signal in the Solar Spectrum (6S), 6S User's Guide Version 2*, NSAS Goddard Space Flight Center, Code 923, Greenbelt, MD.

Vogelmann, J. E. (1988), Detection of forest change in the Green Mountains of Vermont using Multispectral Scanner data. *Int. J. Remote Sens.* 9:1187–1200.

Wen, G., Tsay, S., Cahalan, R. F., and Oreopoulos, L. (1999), Path radiance technique for retrieving aerosol optical thickness over land. *J. Geophys. Res.* 104(D24):31,321–31,332.